Flame capturing with an advection-reaction-diffusion model

Natalia Vladimirova†, V. Gregory Weirs†, and Lenya Ryzhik‡

†ASC/Flash Center, Department of Astronomy & Astrophysics, The University of Chicago, Chicago, IL 60637, USA

‡Department of Mathematics, The University of Chicago, Chicago, IL 60637, USA

Abstract. We conduct several verification tests of the advection-reaction-diffusion flame capturing model, developed by Khokhlov (1995) for subsonic nuclear burning fronts in supernova simulations. We find that energy conservation is satisfied, but there is systematic error in the computed flame speed due to thermal expansion, which was neglected in the original model. We decouple the model from the full system, determine the necessary corrections for thermal expansion, and then demonstrate that these corrections produce the correct flame speed. The flame capturing model is an alternative to other popular interface tracking techniques, and might be useful for applications beyond astrophysics. **(7 March 2005)**

1. Introduction

1.1. Modelling a flame as an interface

For simulations of systems involving flames, several strategies for computing the flame are available. If the flame length scale is not much smaller than the computational domain, then highly detailed kinetics models, high-order discretizations, and adequately posed initial and boundary conditions can be used to probe the structural subtleties of the flame. At the other extreme are flames so much smaller than the computational domain they are impossible to resolve numerically; then the most common approach is to model the flame as a discontinuity in the thermodynamic variables.

A number of techniques dealing with infinitely thin interfaces are available in the literature [12, 9]. Among them are front tracking methods, known for better accuracy; level set methods, which easily treat topological changes; and volume-of-fluid methods, which possess an intrinsic conservation property. All these methods do the essentially the same thing: starting with the current position of the interface and its speed of propagation, compute the position at a later time. Each method strikes a different compromise between computational cost, accuracy, development and implementation cost, and other desirable properties.

However, few applications can take advantage of the commonality among the interface techniques. Users cannot easily swap interface methods in their codes as requirements change – allowing one to use the technique with the best properties for, say, the available computational power, or a new regime of phenomena they want to investigate. When an interface method is incorporated into a physical model, it is encumbered with additional restrictions. For example, the volume of incompatible fluid on both sides of the interface must remain unchanged, or thermodynamic quantities across the flame front must satisfy the Rankine-Hugoniot jump conditions, or a biological interface might set conditions on elasticity or surface charge. The challenge of building a simulation tool involving an interface technique is not in choosing or implementing the technique itself, but in coupling the interface technique with the other physics models.

The biggest challenge in representing a flame as an infinitely thin interface is to correctly model the coupling between the flame speed and thermodynamic conditions on each side of the flame. The difficulty is reduced if the flame speed can be assumed to be independent of thermodynamic states and the fluid on both sides sides of the flame can be assumed incompressible. If these conditions are satisfied, the system can be modelled without reconstructing the interface (without determining the precise location of the interface as it crosses each computational cell,) which permits taking full advantage of the level set approach [11].

However, if the flame speed depends on the local thermodynamics or the incompressibility assumption is invalid, then interface reconstruction is unavoidable [13]. Moreover, modelling a compressible fluid implies solving the energy equation, which introduces another constraint associated with the interface: the transformation of chemical energy to thermal energy must be consistent with the transformation of unburned mass (reactant) to burned mass (product).

1.2. Original ARD model

In 1995 Khokhlov developed a flame model which combines the automatic treatment of interface topology with an energy conservation mechanism [7]. The easy treatment of flame topology follows from an implicit interface representation. Similar to the level set method where the interface is described by a scalar level set variable, the interface in Khokhlov's method is described by a scalar reaction progress variable. The value of the reaction progress variable is zero in the reactant, one in the product, and monotonically varies inside a "flame region." The width of the flame region is much larger than the thickness of the physical flame it represents; it is set by the model to be several computational zones thick.

Unlike the level set variable, which in the vicinity of the flame is interpreted as the signed distance to the interface, but far from the interface has no physical meaning, the reaction progress variable is relevant everywhere. It can be associated with the mass fraction of burned material in a cell. In this way, the reaction progress variable is similar to the volume fraction variable in the volume of fluid method. But contrary to the volume fraction variable, the reaction progress variable distributes the interface over several computational cells.

The evolution of the reaction progress variable is described by the advection-reaction-diffusion (ARD) equation. The reaction progress variable is advected by the flow, diffuses, and is generated in some simple source term, here called reaction. In the limit of fast reaction rate and small diffusivity (thin flame limit) the advection-reaction-diffusion equation is equivalent to the level set equation and describes the front governed by Huygens's principle [6, 10]. The front's speed of propagation with respect to the flow field depends on diffusivity and reaction rate. In Khokhlov's model, however, diffusivity and the reaction rate have very little to do with the physical properties of the fluid. They are artificial parameters chosen with the sole purpose of producing a desired flame speed and front thickness.

The ARD equation is added to a system of equations representing other types of physics, e.g. the Euler equations with a suitable state equation. The ARD model "gets input from physics" through the advection velocity and the flame speed, which can be determined dynamically from the local conditions. The flame model is coupled back to the flow field through a source term in the energy equation: the amount of burned material, and consequently the energy released, is proportional to the change in reaction progress variable.

1.3. Extending the ARD model

The original ARD model was designed to represent deflagrations in a white dwarf star, as an initial stage of a Type Ia supernova explosion. Although the fluid in the burned and unburned regions cannot be assumed incompressible because of strong gravitational stratification, the local conditions in the vicinity of the flame are almost incompressible. Near the center of the white dwarf, the thermonuclear flame is extremely thin (10^{-8} – 10^{-6} of the star radius), highly subsonic, and is characterized by a small density decrease across the flame (about 10%), and essentially no jump in pressure (less than 1%) [16].

To extend the model to the compressible regime, modifications are required to account for velocity variations on the scale of the interface thickness. Velocity variations come from the density jump between unburned and burned fluids: when material crosses the flame front it expands and accelerates, resulting in normal velocity variations of the order of the flame speed. The original method was built on the implicit assumption that these velocity variations do not affect the travelling wave speed; the control parameters for the model were chosen based on the properties of the isolated ARD equation (discussed in Sec. 2.) Consequently the original ARD model fails to recover the proper flame speed unless thermal expansion is negligible.

Our solution to this problem is based on a physical interpretation of the ARD equation, which allows us to decouple it from the mass, momentum, and energy equations. This approach is described in Sec. 3. We can then study the ARD equation in isolation to find the effect of thermal expansion and consequent velocity variation on the flame speed, as explained in Sec. 4. Knowing the effects of thermal expansion, we suggest modifications to the control parameters of the flame capturing model in Sec. 5. With the modifications, the model recovers the desired flame speed, as demonstrated through verification tests in Sec. 6. Section 7 gives suggestions regarding the model's use and implementation and potential avenues for improvement.

2. Properties of the advection-reaction-diffusion equation

The evolution of the reaction progress variable ϕ is described by the advection-reaction-diffusion equation,

$$\phi_t + \mathbf{v} \cdot \nabla\phi = \kappa\nabla^2\phi + \frac{1}{\tau}R(\phi). \tag{1}$$

Here, κ is the diffusion coefficient, τ is the reaction time, and $R(\phi)$ is some simple non-dimensional function of the non-dimensional reaction progress variable ϕ. The reaction progress variable is scaled so that $\phi = 0$ and $\phi = 1$ represent pure reactant and pure product, respectively.

In the absence of advection, the velocity $\mathbf{v} = 0$, and the ARD equation describes travelling wave solutions. For a given reaction rate, $R(\phi)$, the travelling wave speed s_0 is determined by the reaction time τ, and the diffusion coefficient κ. In cases when the dependence $R(\phi)$ is simple enough, the travelling wave speed can be obtained analytically.

One reaction rate for which the analytical front propagation speed is known is the Kolmogorov-Petrovskii-Piskunov (KPP) reaction rate [8, 5],

$$R(\phi) = \frac{1}{4}\phi(1 - \phi). \tag{2}$$

When the KPP reaction rate is inserted in the advection-free equation (1), the analytic solution yields a travelling wave speed $s_0 = \sqrt{\kappa/\tau}$. The KPP reaction rate is often used as a source term in advection-reaction-diffusion models because it makes such models more accessible for rigorous analysis (see reviews [17, 1]).

Another reaction rate we consider is a reaction rate of "ignition" type, where reaction is impossible until the reaction progress variable reaches some critical value, i.e. $R(\phi) = 0$ for $\phi < \phi_0$. Ignition–type reaction terms are widely used to model combustion processes (see review [17]), in particular, for approximating the behavior of Arrhenius-type chemical reaction rates. The original ARD flame-capturing method [7] was developed with a reaction rate of ignition type, specifically, the top-hat reaction rate:

$$\begin{aligned} R(\phi) &= 0, & \phi &< \phi_0, \\ R(\phi) &= R_0, & \phi_0 \le \phi &< 1, \\ R(\phi) &= 0, & \phi &\ge 1, \end{aligned} \tag{3}$$

where R_0 is a constant chosen such that the travelling wave speed is $s_0 = \sqrt{\kappa/\tau}$. (For an arbitrary reaction rate, $s_0 = \sqrt{\kappa/\tau}$ can always be achieved by multiplying the reaction rate by a constant.) In Appendix 1 we show the analytical solution of equation (1) with the top-hat reaction rate and $\mathbf{v} = 0$, and derive the expression for R_0.

Another parameter, which can be constructed from κ and τ, has the dimension of length. We call it the reaction length scale $\delta_0 = \sqrt{\kappa\tau}$. This length scale characterizes the interface thickness, the distance over which ϕ changes from zero to one. Although always of the order of δ_0, the actual interface thickness depends on the particular reaction rate. For instance, the top-hat reaction region is wider than the KPP reaction region with the same diffusivity and the same reaction time, and consequently, the same δ_0. To make comparison between KPP and top-hat reaction rates easier, for each reaction rate we define the interface thickness,

$$l_{\mathrm{kpp}} \equiv 16\delta_0 \qquad \text{and} \qquad l_{\mathrm{tophat}} \equiv 4\delta_0. \tag{4}$$

Defined this way, the two interface thicknesses match, $l_{\mathrm{kpp}} \approx l_{\mathrm{tophat}}$.

In the presence of a non-trivial velocity field, $\mathbf{v} \neq 0$, the reaction front moves with respect to the background flow with some speed s. The relationship between s_0 and s depends on the velocity field. If the spatial variation of the velocity field is weak in comparison with s_0, then $s = s_0$. Larger velocity variations redistribute the reaction progress variable and alter the front speed. A great deal of effort has been spent in deducing the relationship between s and s_0 for turbulent velocity fields, which we will not review here.

Our goal is to solve the ARD equation as one member of a system of equations, in which the velocity field is computed as part of the solution. In the fully coupled system, exothermic reaction in the flame causes a reduction in the density, i.e. thermal expansion. Mass conservation then requires acceleration of the fluid as it passes through the flame, with consequent alteration of the flame speed.

In the next section, we will derive an expression for the velocity profile across the fully coupled flame as a function of the reaction progress variable. Then, using this velocity profile, we will study the ARD equation in isolation. We will show that for a given density ratio, the flame speed and the flame thickness depend on the diffusion coefficient and the reaction time, and we will determine the dependencies,

$$s = s(\kappa, \tau) \qquad \text{and} \qquad l = l(\kappa, \tau). \tag{5}$$

Finally, a comment about terminology and notation. When the velocity profile accounts for thermal expansion, we call s the *variable-density* flame speed. The spatially-constant velocity field does not account for thermal expansion, so we can refer to s_0 as the *isochoric* flame speed. The quantities s_0 and δ_0 are not directly relevant to the variable-density case, but we still use them as reference quantities,

$$s_0 \equiv \sqrt{\kappa/\tau} \qquad \text{and} \qquad \delta_0 \equiv \sqrt{\kappa\tau}, \tag{6}$$

based on diffusivity and reaction time.

3. Coupling advection-reaction-diffusion flame model to flow physics

A natural way to couple the ARD flame equation to the flow physics comes from the physical interpretation of the reaction progress variable as the mass fraction of the product. If the rate of conversion from reactant to product is $\rho\dot{\phi}$, and q is the energy released per unit mass of converted fluid, an additional heat release term appears in the energy equation. Then the full system of governing equations becomes,

$$\begin{aligned}
&\frac{\partial \rho}{\partial t} + \nabla \cdot (\rho \mathbf{v}) = 0, \\
&\frac{\partial \rho \mathbf{v}}{\partial t} + \nabla(\rho \mathbf{v}\mathbf{v}) + \nabla P = \mathbf{f}, \\
&\frac{\partial \rho E}{\partial t} + \nabla \cdot [(\rho E + P)\mathbf{v}] = \mathbf{v} \cdot \mathbf{f} + q\rho\dot{\phi}, \\
&\frac{\partial \rho \phi}{\partial t} + \nabla \cdot (\rho \phi \mathbf{v}) = \rho\dot{\phi}, \\
&\qquad\qquad \dot{\phi} = \kappa \nabla^2 \phi + \frac{1}{\tau} R(\phi).
\end{aligned} \tag{7}$$

Here, $\rho E = \rho e + \frac{\rho \mathbf{v}\mathbf{v}}{2}$ is the total energy and $e = e(\rho, P)$ is specific thermal energy, where the functional relationship is specified by the equation of state. Note that by substituting $\rho\dot{\phi}$ from the equation for reaction progress variable into the energy conservation equation, we obtain the conservation of energy $\rho E' = \rho(e - q\phi) + \frac{\rho \mathbf{v}\mathbf{v}}{2}$. The ARD equation influences the rest of the system through the energy source term, while the flow equations influence the ARD equation through the velocity field. Treating the convection of burned mass in strong conservation form, rather than solving equation (1) directly, allows a consistent numerical discretization of the left hand sides of all equations in the system (7).

Recall that the advection-reaction-diffusion equation was introduced to system (7) solely for modeling the flame. The flame speed, s, the flame thickness, l, and the heat release, q, are input parameters in the flame capturing model. The diffusion coefficient κ and the reaction timescale τ in the ARD equation are not related to the physical diffusion or reaction, but chosen solely to produce a desired flame speed and a specified flame width. For a given flame speed and flame thickness, the diffusion coefficient and the reaction timescale can be found from relations (5),

$$\kappa = \kappa(s, l) \qquad \text{and} \qquad \tau = \tau(s, l). \tag{8}$$

If all goes well, the observed flame speed $\hat{s}$ and thickness $\hat{l}$ will be the same as the input s and l.

Unfortunately, at this point relations (5), and consequently (8), are available only for an isochoric flame. Extension to the compressible regime requires the velocity profile across the flame interface as function of the reaction progress variable, which we develop next.

We consider a one-dimensional laminar flame with no external force applied to the fluid. We assume the system (7) has reached a stable travelling wave solution. Then, in the reference frame of the travelling wave, the mass, momentum, and energy conservation equations have a simple algebraic form:

$$\begin{aligned} &\rho v = const, \\ &\rho v^2 + P = const, \\ &v\left(\rho(e - q\phi) + P + \frac{\rho v^2}{2}\right) = const. \end{aligned} \tag{9}$$

Equations (9) are generalized Rankine-Hugoniot conditions for a partially burned fluid; equating states for $\phi = 0$ and $\phi = 1$, we obtain the usual Rankine-Hugoniot jump conditions for pressure, density, and normal velocity across the interface.

Equations (9) with the equation of state implicitly parameterize the local state (ρ, P, v) as a function of the unburned state (ρ_u, P_u, v_u) and the reaction progress variable,

$$\begin{aligned} \rho &= \frac{\rho_u}{\tilde{\alpha}(\phi)}, \\ v &= v_u - s\left(\tilde{\alpha}(\phi) - 1\right), \\ P &= P_u - \rho_u s^2 \left(\tilde{\alpha}(\phi) - 1\right). \end{aligned} \tag{10}$$

Here $\tilde{\alpha}(\phi)$ is the ratio of the (partially burned) fluid density to the unburned fluid density and is a function of the reaction progress variable only.

The functional relationship $\tilde{\alpha}(\phi)$ depends on the equation of state. For instance, for the gamma-law equation of state, $e = \frac{1}{\gamma-1}\frac{P}{\rho}$, and one can derive

$$\tilde{\alpha}(\phi) = 1 + \frac{1}{\epsilon_1}\left(1 - \sqrt{1 - 2\epsilon_1\epsilon_2\phi}\right), \tag{11}$$

$$\text{with} \qquad \epsilon_1 = (\gamma + 1)\,\frac{s^2}{c_u^2 - s^2}, \qquad \epsilon_2 = (\gamma - 1)\,\frac{q}{c_u^2 - s^2},$$

where $c_u = \sqrt{\gamma P_u/\rho_u}$ is the speed of sound in the unburned fluid.

For a highly subsonic flame, $s \ll c_u$ and consequently $\epsilon_1 \ll 1$. Then (11) is linear in ϕ, $\tilde{\alpha}(\phi) = 1 + \epsilon_2\phi$, and the velocity profile is linear:

$$v(\phi) = v_u + \phi\Delta v_f, \tag{12}$$

where $\Delta v_f = -(\alpha - 1)s$ is the velocity change across the flame, and α is the density ratio of unburned and burned fluids, $\alpha = \rho_u/\rho_b = \tilde{\alpha}(1) \approx 1 + \epsilon_2$. Expression (12) assumes a one-dimensional flame propagating to the right, but can be generalized to the multi-dimensional case, $\mathbf{v}(\phi) = \mathbf{v}_u + \mathbf{n}\,\phi\Delta v_f$, where $\mathbf{n}$ is the unit normal to the front pointing in the direction of flame propagation. Note that no assumptions have been made on ϵ_2, i.e. the parameter $\epsilon_2 \approx \frac{\gamma-1}{\gamma}\frac{q\rho_u}{P_u}$ need not be small.

The velocity jump Δv_f is a direct consequence of thermal expansion. Thermal expansion influences the flame speed through two competing effects. On one hand, the burned fluid moves away from the flame at a greater velocity, and this slows the flame. On the other hand, expansion thickens the reaction zone, which increases the amount of fuel burned per unit time; consequently the flame speed is increased. To show these competing effects, we integrate the one-dimensional form of the ARD equation in (7) or the equivalent isolated ARD equation (1), with the velocity profile in (10), and solve for the flame speed, obtaining

$$s = s_0 \frac{\int_{-\infty}^{+\infty} R\ d(x/\delta_0)}{\int_0^1 \frac{\rho_u}{\rho(\phi)}\, d\phi},$$

where s_0 and δ_0 are defined in (6). Compared to the isochoric case, the burning region in the variable-density case is wider, leading to a larger integral in the numerator. At the same time, the ratio $\rho_u/\rho(\phi)$ is always greater than one, so the integral in the denominator is also larger. The difference between s and s_0 depends both on the distribution of $\phi(x)$ across the interface and the density dependence $\rho(\phi)$ on the reaction progress variable. In general, the variable-density flame speed can be larger or smaller than the isochoric flame speed.

For a general equation of state, an analytic expression for $\tilde{\alpha}(\phi)$ might not be available, but simplifications might still be possible. In the zero Mach-number limit, kinetic energy can be neglected in (9). This implies the pressure is constant across the flame, and the energy equation reduces to a purely thermodynamic relation. Thus, the state at any stage of reaction (at any ϕ) can be found from any known state by solving

$$\begin{aligned} &e(\rho, P) + \frac{P}{\rho} - q\phi = const, \\ &P = const. \end{aligned} \tag{13}$$

Equations (13) provide an approximation for the local expansion coefficient $\tilde{\alpha}(\phi)$, and from $\tilde{\alpha}(\phi)$ and mass conservation (10), the local velocity, $v(\phi)$. The ability to estimate the burned and unburned states from a local state is also useful, e.g. if the flame speed, as an input to (8), depends on conditions on both sides of the interface.

By analyzing the flame profile for the full system, we have determined the effect of thermal expansion on the velocity, i.e. $v(\phi)$. Knowing $v(\phi)$, we can analyze thermal expansion and its effect on the flame speed considering only the ARD equation — a much simpler task than analyzing the full system. While we have used this technique for accessing the role of thermal expansion, the approach could be used for other complex phenomena. The key idea is to express some aspect of the complex behavior in the full system through the dependence of the velocity on the field variable in the ARD equation. The nonlinear velocity captures the coupling of the full system to the ARD equation. While the ARD equation has been studied with prescribed velocity fields representative of, e.g. turbulent velocity fluctuations, we are not aware of the use of the velocity to represent thermodynamic phenomena, or the specification of the velocity as a function of the field variable.

4. Numerical solution of isolated ARD equation with ϕ-dependent velocity

Now that we have derived an expression (12) for $v(\phi)$ we return to the solution of equation (1) with an advection velocity which accounts for thermal expansion.

For some simple reaction rates the variable-density flame speed can be found analytically. The KPP reaction rate (2) has a single stable point, $\phi = 1$, and metastable point, $\phi = 0$, and is characterized by the condition that the function $R(\phi)$ is positive and convex on the interval $0 < \phi < 1$. In Appendix 2 we show that if the velocity is as in (12), there is only one way to connect metastable and stable points on the phase diagram $(\phi, \dot{\phi})$. The solution corresponds to the flame speed $s = s_0$ for any $\Delta v_f < 0$.

Unfortunately, the analytical approach above does not extend to reaction rates with multiple stable and unstable points, and thus cannot be used for reaction rates of "ignition" type, such as the top-hat reaction rate (3). In this section we solve the ARD equation (1) numerically, using the ϕ-dependent advection velocity (12). This exercise has two purposes.

First, we want to verify the independence of the flame speed on the jump Δv_f for the KPP reaction rate, and to measure the effect of the jump for the top-hat reaction rate. Doing so, we will consider well-resolved numerical solutions of equation (1).

Second, we want to study the effect of spatial resolution. In the flame-capturing model, the ARD equation is used at low spatial resolutions to mimic the discontinuity. Keeping the front thin reduces the effect of background velocity and thermodynamic variations, which are unavoidable in the full system and which might modify the internal flame structure. At the same time, we will keep the time step significantly smaller than both diffusive and advection CFL limits, assuming that in a compressible flow simulation the time step is set by the CFL condition based on the speed of sound. The small time step ensures that numerical errors due to temporal discretization are dominated by spatial discretization errors.

We discretize equation (1) using fourth-order central differences in space and the explicit Euler method in time. The fluid velocity profile is specified by (12). The KPP reaction rate is given in (2) and the top-hat rate in (3). We express resolution in terms of computational cells across the reacting region, $b = l/\Delta x$, where l is the width of the isochoric flame (4). The time step is typically $\Delta t = 10^{-3}\tau$, which is at least two orders of magnitude smaller than the diffusive and advection CFL limits. We repeated a number of cases with different time step sizes and using the 3rd-order Adams-Bashforth time advancement algorithm and obtained essentially the same results.

To find the effect of thermal expansion, we first conduct simulations for an isochoric fluid, $\Delta v_f = 0$, then for an expanding fluid with $\Delta v_f = -s_0$. To test the influence of the simulation reference frame, we consider three velocities in the unburned gas: $v_u = -s_0$, $v_u = 0$, and $v_u = +s_0$. If the flame speed were not affected by thermal expansion, then $\Delta v_f = -s_0$ would correspond to a density ratio of $\alpha = 2$, and the background velocity $v_u = -s_0$ would place the expansion-independent flame stationary in the observer's frame of reference. The second value, $v_u = 0$, corresponds to the reference frame with stationary reactant, and finally, $v_u = s_0$, corresponds to the frame with stationary product. Of course, if the flame speed is influenced by thermal expansion, then the flame, reactant, and product will not remain stationary in the respective reference frames.

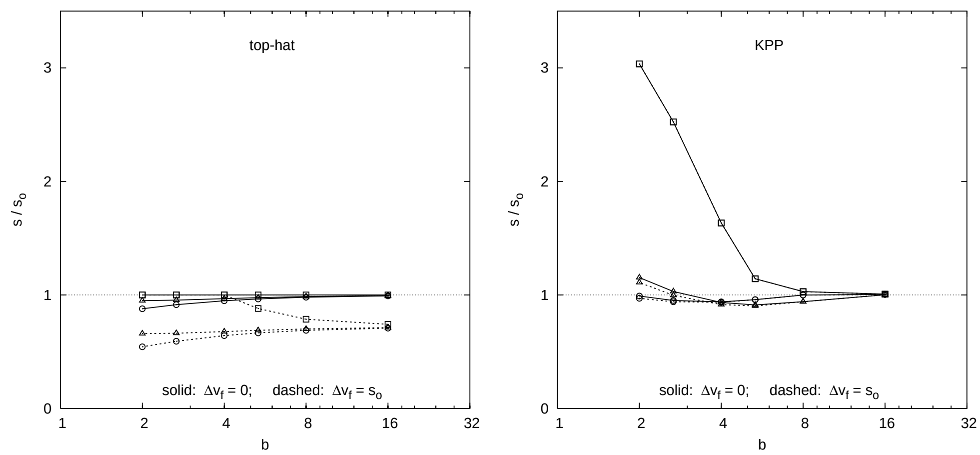

Figure 1. Dependence of the travelling wave speed on resolution and simulation reference frame. Reaction rates: top-hat, left; KPP, right. Simulation reference frame: $v_u = -s_0$, squares; $v_u = 0$, circles; $v_u = s_0$, triangles. Solid line corresponds to isochoric case ($\Delta v_f = 0$) and dashed line corresponds to variable-density case ($\Delta v_f = -s_0$).

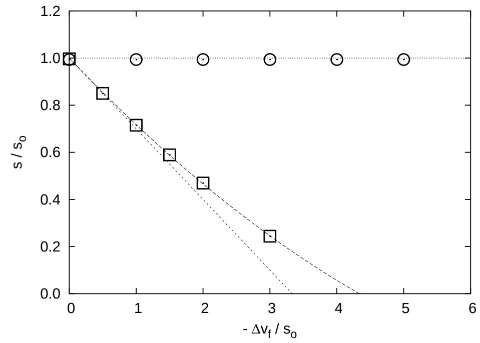

Figure 2. The travelling wave speed as function of expansion parameter Δv_f. Reaction rate: KPP, circles; top-hat, squares. The dashed line shows the approximation with quadratic function, $s/s_0 = 1 - k_1(-\Delta v_f/s_0) + k_2(-\Delta v_f/s_0)^2$, where $k_1 = 0.2982$ and $k_2 = 0.0156$. The dotted line shows the linear approximation, $s/s_0 = 1 - 0.3(-\Delta v_f/s_0)$. Simulations were performed in the reference frame of the unburned fluid, $v_u = 0$, at resolution $b = 32$.

The flame speed, s, measured for the isochoric and variable-density cases, is shown in Fig. 1. As resolution increases, the flame speed for the KPP reaction rate converges to $s = s_0$ for both cases. This confirms the flame speed is independent of the expansion parameter Δv_f, for the KPP rate. For the top-hat reaction rate, the flame speed converges to $s = s_0$ in the isochoric case. However, the variable-density flame speed converges to $s = 0.72 s_0$, independent of the reference frame. Next we quantify the difference between the isochoric and variable-density flame speeds as a function of the expansion parameter.

We have measured flame speeds for several different different values of Δv_f at high resolution. The results for both top-hat and KPP reaction rates are shown in

Fig. 2. As expected, the flame speed for the KPP rate does not depend on Δv_f. For the top-hat reaction rate and small jump Δv_f, the flame speed can be approximated by a linear function. The expressions,

$$\begin{aligned} &\text{KPP:} && s = s_0, \\ &\text{top-hat:} && s \approx s_0 + 0.3\Delta v_f, \end{aligned} \tag{14}$$

summarize our analytical and numerical study of the isolated ARD equation for velocity profiles which account for thermal expansion.

Advection against the flame ($v_u = -s_0$) at low resolutions is challenging for the numerical scheme for both KPP and top-hat reaction rates, but especially for KPP. We observe that oscillations precede the front and begin to burn, increasing the effective flame speed. It can be shown that without the reaction term, discretizing the advection term with central differences implies a limit on the cell Reynolds number $|v|\Delta x/\kappa < 1/2$, the violation of which results in an oscillatory solution [15]. The derivation in [15] is for the advection-diffusion equation, discretized with second-order central differences, and the value (1/2) of the limit is specific to that discretization. Nevertheless, we noticed a strong correlation between resolution and velocity and the appearance of oscillations in the flame front, with corresponding errors in the flame speed.

For the ARD equation, the above cell Reynolds number constraint for the advection-diffusion equation can be expressed in terms of the number of grid points per interface. Note that we use fourth-order differences, so these are just estimates. We obtain $b \geq 8|v|/s_0$ for the KPP reaction rate, and $b \geq 2|v|/s_0$ for the top-hat reaction rate. The coefficient in front of $|v|/s_0$ depends on reaction rate because of our definition of the flame front resolution, b. Recall that to match the flame thicknesses for the different rates we specified (4), so that at the same resolution, the diffusion coefficient for the KPP flame is one-fourth that for the top-hat flame.

One way to avoid the restriction on the cell Reynolds number is to use an upwind discretization of the scheme advection terms. In later sections we will show results obtained with such a scheme, PPM, and we will see that it delivers much better results for the under-resolved cases.

5. Input parameters for flame capturing model

Analyzing the isolated ARD equation in the previous section, we treated the flame speed as an output of the problem. We wanted to know how s depends on the model parameters: diffusion coefficient κ, reaction timescale τ and the velocity jump Δv_f. To use the ARD equation as a flame-capturing model, we want to solve the inverse problem. We want to specify s as an input and compute the corresponding model parameters; if the model behaves correctly, then the observed flame speed $\hat{s}$ in our simulations will be the same as the input flame speed s.

The parameters for the flame capturing model can be calibrated using (14), which expresses the dependence of s on Δv_f. Recall that in the full system, the velocity jump is due to thermal expansion and is directly related to the the density ratio. Substituting $\Delta v_f = -(\alpha - 1)s$ in (14) and solving for the flame speed, we obtain $s = s_0/a$, where

$$\begin{aligned} &\text{KPP:} && a = 1, \\ &\text{top-hat:} && a = a(\alpha) \approx 1 + 0.3(\alpha - 1). \end{aligned}$$

Thus, we express the flame speed in terms of density ratio α, a more accessible quantity than the velocity jump across the interface. Next, using the definitions (6) we obtain the diffusion coefficient and the reaction time,

$$\kappa = as\delta_0, \qquad \tau = \delta_0/(as). \tag{15}$$

The length scale δ_0 is related to the isochoric flame thickness as in (4). The variable-density flame thickness is usually larger than the isochoric flame thickness. (We could calibrate the parameters to match the flame thickness, as well as the speed, but have not done so.)

This section concludes our modifications to the ARD flame capturing model. In comparison to the original ARD model, we have added a calibration factor to the mapping of s and δ_0 to κ and τ. This factor accounts for the effect thermal expansion on the flame speed. We have empirically determined the dependence of s on the density change across the flame for the top-hat rate (Fig. (2),) and the corresponding calibration factor, valid for small density jumps. We have also analytically and numerically demonstrated that for the KPP reaction rate, the calibration is not needed because the flame speed is insensitive to thermal expansion.

In the next section we will demonstrate that with our calibration, the flame-capturing model with the top-hat rate is effective.

6. Verification of the model

The results above were obtained with a "prototype" code, which solves the isolated ARD equation for a prescribed velocity field. To verify the coupling with the compressible flow equations, we implemented the ARD flame capturing model in the `FLASH` code [4, 2], a multidimensional, multiphysics, block-structured AMR code primarily intended for astrophysical applications.

The `FLASH` code solves the system (7) using timestep splitting. The piecewise parabolic method (PPM) advances the solution in time accounting for the convective terms [3], and directional splitting is used whenever multiple spatial dimensions are considered [14]. Then a second step is taken for the diffusion and reaction terms; these operators are treated in an unsplit (in time) fashion and advanced using the first-order explicit Euler method. Second-order central differences are used for the diffusion term.

The ARD flame capturing model was implemented and tested in 1-, 2-, and 3-D Cartesian, 2-D cylindrical, and 3-D spherical coordinates. The `FLASH` code is a structured AMR code, but the flame-capturing model was implemented assuming the ARD flame is always discretized at the finest refinement level. In the tests we performed, derefining the grid outside of the flame region did not directly affect the performance of the flame-capturing model.

Several equation of state (EOS) models are implemented in `FLASH`. Here we show the results obtained using the gamma-law EOS; we have performed similar tests with the Helmholtz EOS (commonly used for degenerate stellar interiors) and did not find any unexpected differences.

6.1. Planar flame: test of concept

This section contains a set of one-dimensional tests of the ARD flame capturing model in Cartesian coordinates. The goal is to verify that the flame model still performs its function, i.e. propagates the flame at the desired speed, when coupled to the Euler

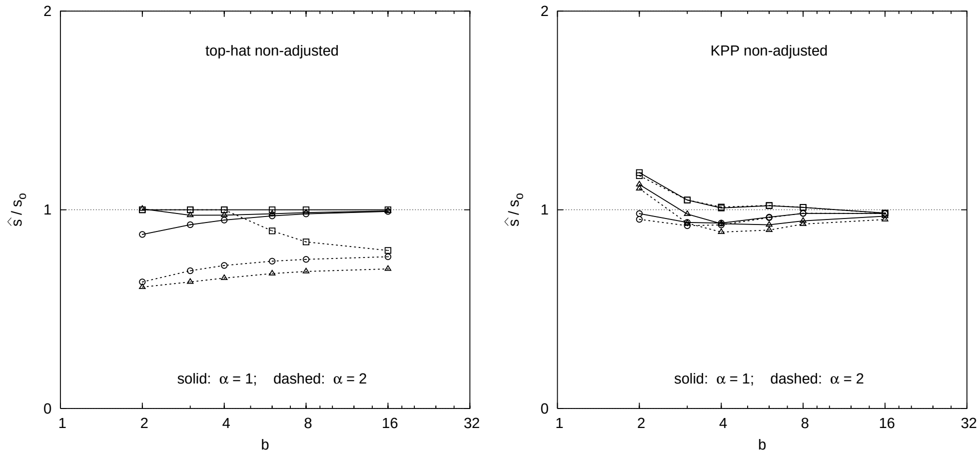

Figure 3. Dependence of the travelling wave speed on resolution for top-hat (left) and KPP (right) reaction rates and different advection velocities $v_u = -s_0$ (squares), $v_u = 0$ (circles) and $v_u = s_0$ (triangles). Solid lines correspond to isochoric case ($\alpha = 1$) and dashed lines correspond to variable-density case ($\alpha = 2$). The results were obtained without adjustment for compressibility effects ($a = 1.0$).

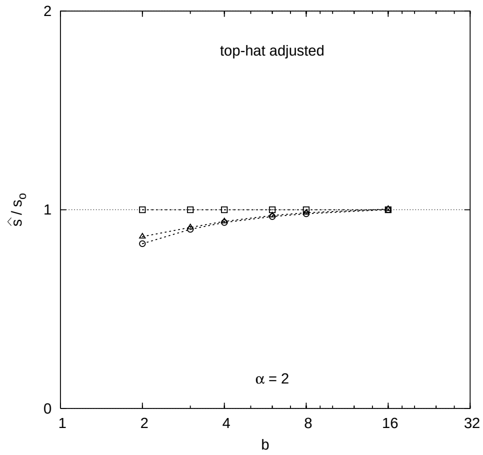

Figure 4. Travelling wave speed for top-hate reaction rate shown in Fig. 3, computed with adjustment for compressibility effects ($a = 1.3$).

equations. The physical conditions are chosen to match the simulations discussed in Sec. (5), in which the ARD equation (1) was solved in isolation.

Given the unburned state and the flame speed, we can control the density ratio α by choosing the heat release q. If $q = 0$, then $\alpha = 1$, and the ARD equation is decoupled from the Euler equations in (7). In this case, the only difference between system (1) and system (7) is the difference in the numerical method, i.e. between central differences and PPM advection schemes.

Choosing the heat release so that $\alpha = 2$ is equivalent to setting $\Delta v_f = -s_0$ in (12). Recall that when $q \neq 0$, (12) is an approximation which relies on several physical

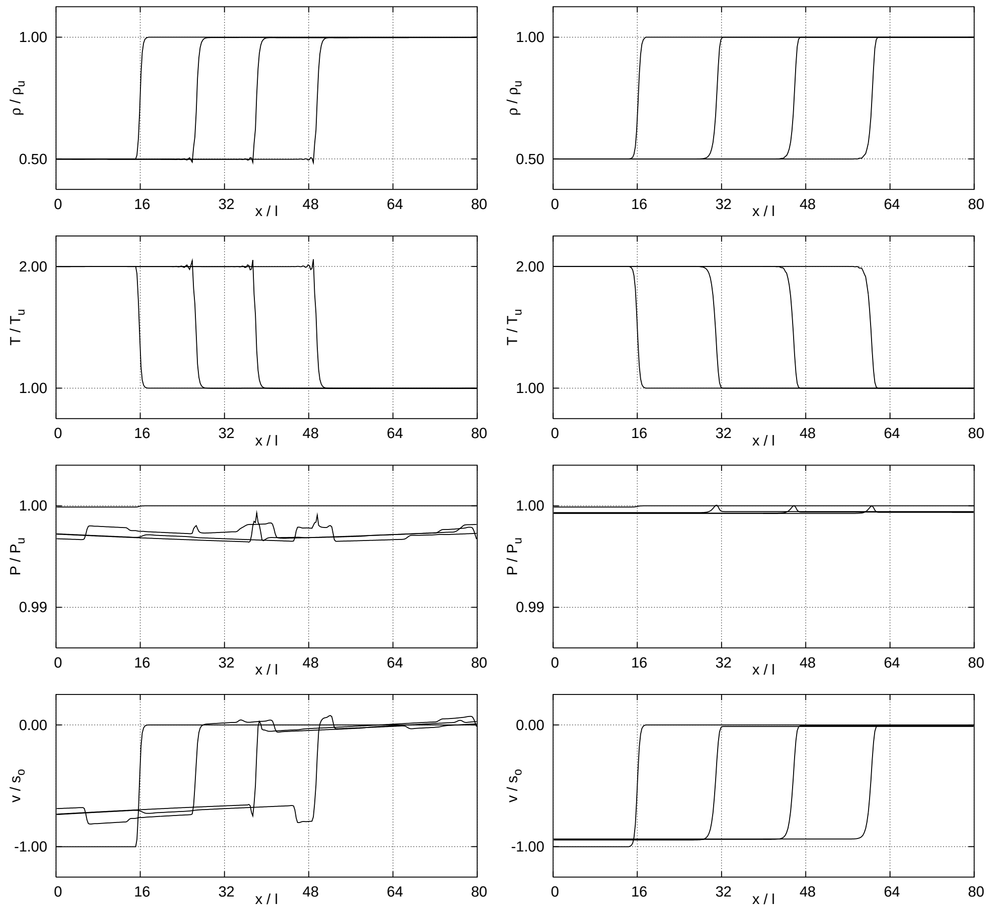

Figure 5. Density, temperature pressure, and fluid velocity profiles across the ARD flame front, computed using top-hat (left) and KPP (right) reaction rates. The expected position of the front and theoretical values of the pre- and post-flame quantities are marked with dotted lines. The results were obtained for resolution $b = 4$ and without adjustment for compressibility or resolution effects ($a = 1.0$).

assumptions, and the correspondence between solutions of (1) and (7) depends on how well those assumptions are satisfied, as well as the difference between numerical methods.

Figure 3 plots the measured speed $\hat{s}$ of the coupled ARD flame (solution of (7)) in the same way as Fig. 1 does for the isolated ARD equation (1). As before, we want to determine the influence of the resolution, the advection velocity, and different reaction rates. For the top-hat reaction rate the results for isolated and coupled ARD equations agree. For the KPP-type reaction, the results agree except at low resolution for negative advection velocity (flame propagation against the flow.) In this regime PPM has an advantage over central differences; oscillations generated at the flame due to low resolution are damped by PPM's numerical viscosity.

As for the isolated ARD flame, the flame speed is underpredicted for the coupled

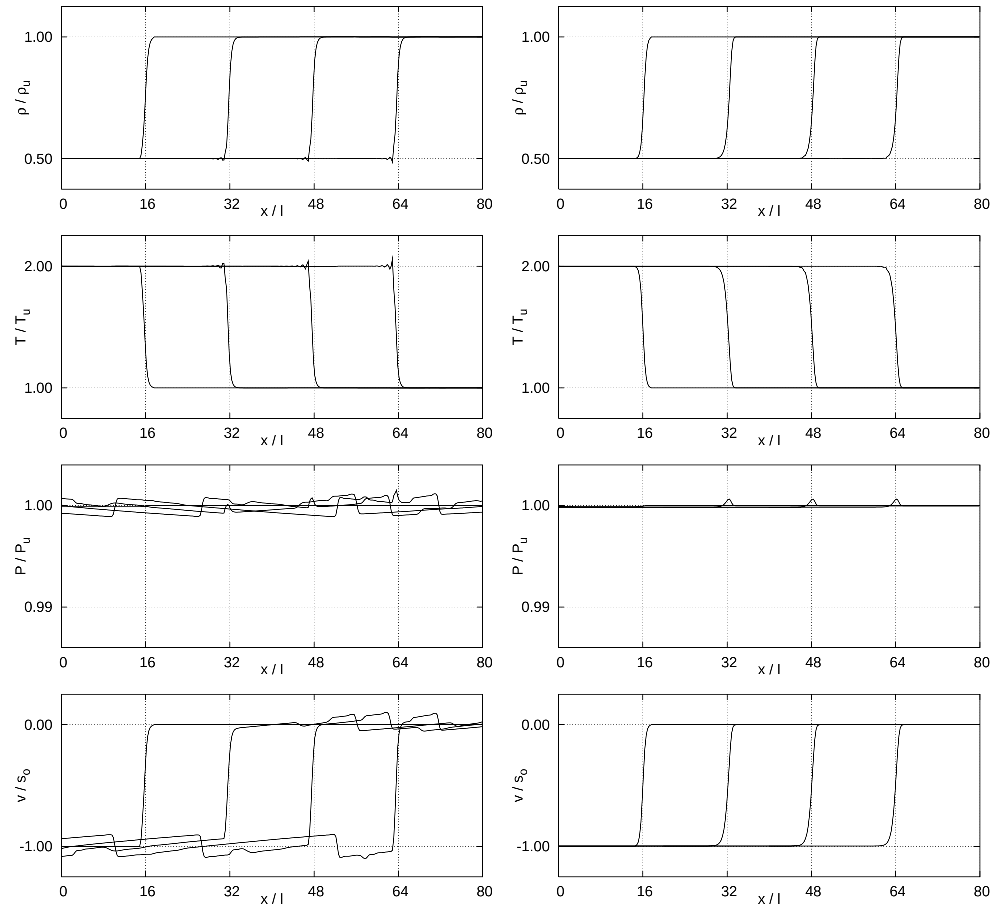

Figure 6. Profiles from Fig. (5), computed with adjustments for compressibility and resolution effects, top-hat on the left ($a = 1.38$) and KPP on the right ($a = 1.07$).

ARD flame when the top-hat reaction rate is combined with thermal expansion (Fig. 3). Setting the adjustment coefficient to $a = 1.3$, according to equation (15), improves the computed flame speed as expected (Fig. 4).

The profiles of the thermodynamic quantities and fluid velocity across the flame front are shown for simulations without and with the adjustment for thermal expansion in Fig. 5 and Fig. 6, respectively. Note that in Fig. 6 we also include a small adjustment for both reaction rates to compensate for inaccuracies due to low resolution. This adjustment is treated in the same way as thermal expansion. The jumps in density and temperature are well represented by the flame model, whether or not the adjustments are included, indicating that even if the flame speed is predicted poorly, the correct amount of energy (due to reaction) is deposited across the interface.

There are several points to make about the velocity profiles. The location and magnitude of the velocity jump across the flame are both dependent on the computed flame speed; for the dependence of the magnitude, see the equation for v in (10), evaluated at $\phi = 1$. In Fig. 5, the velocity jump is smaller than expected because

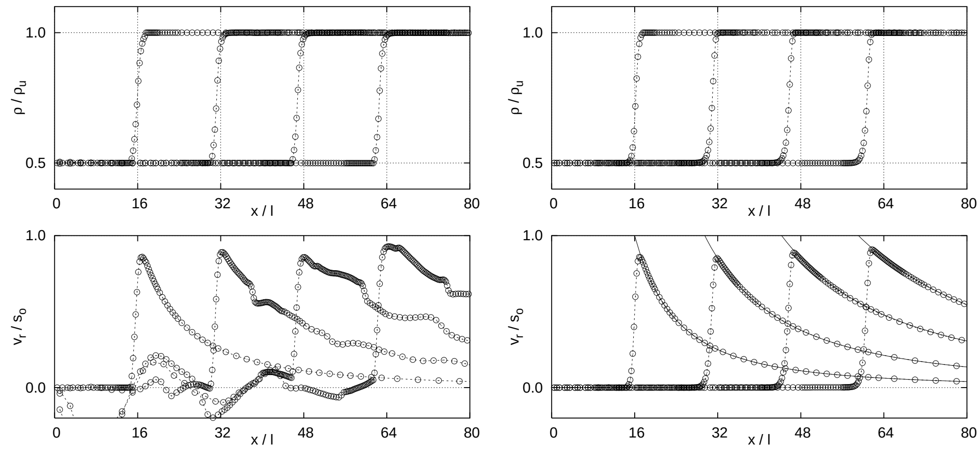

Figure 7. Density (top) and radial velocity (bottom) for spherical flame at four different times, computed in 1-D spherical coordinates for top-hat (left) and KPP (right) reaction rates. Theoretical velocity corresponding to the flame at current location is shown with solid line.

the flame speed is underpredicted. When the adjusted speed is used, Fig. 6 shows the correct velocity jump is recovered. When the top-hat reaction rate is used, the velocity profile is much less smooth compared to the KPP rate. The "noise" is actually acoustic in nature, and is ultimately due to the discontinuous form of the top-hat rate. Close examination of consecutive time steps reveals that as the reaction progress variable in an unburned computational cell increases above ϕ_0, the instantaneous change in the thermodynamic state initiates an acoustic pulse which propagates both upstream and downstream of the flame front. The strength of the pulse decreases with increasing resolution because the total energy release is spread over more cells, and the relative energy release for a cell just beginning to burn is smaller. Without smoothing the discontinuities in the top-hat rate, these pulses are unavoidable. The small, localized, post-shock oscillations in density and temperature are also due to the discontinuities in the top-hat rate.

For the KPP rate, the slight bump in the pressure through the flame is due to slight errors in the flame structure. The pressure is computed from the density and energy, and it is actually a slight error in the density profile, imperceptible on the scale of the density jump across the flame, which results in the bump in the pressure. The key points to make about these errors in the KPP flame structure are that they are small, self-consistent, highly localized to the interface itself, and benign — the global solution remains unaffected and unpolluted.

6.2. Spherical flame: geometry test

We use a spherical flame to test the flame-capturing model in different coordinate systems. Because of its simplicity, the spherical flame has a known theoretical solution.

The theoretical solution describes an infinitely thin flame [18], which starts from an infinitely small hot spot in an otherwise uniform, motionless fluid. Since there is no length scale involved in the problem, the solution at $t > 0$ is self-similar with respect

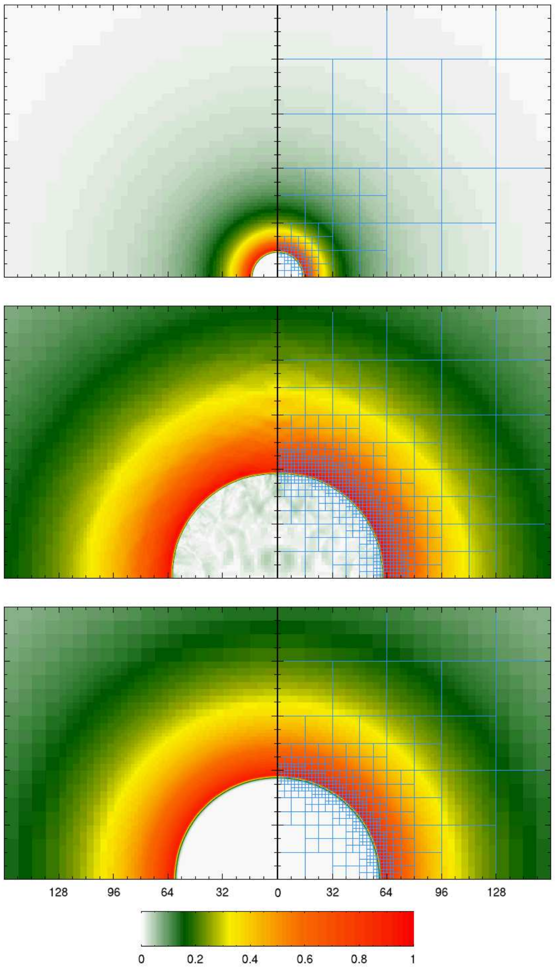

Figure 8. Radial velocity in for spherical flame computed in 2-D cylindrical coordinates. From top to bottom: initial velocity, $t = 16l/(\alpha s) \equiv t_0$; velocity at $t = 4t_0$, top-hat reaction rate; velocity at $t = 4t_0$, KPP reaction rate. Distance is shown in units of l, and velocity in units of s.

to the flame position $r_f = \alpha st$,

$$
\begin{aligned}
&r < r_f : \\
&\qquad \rho = \alpha\rho_u, \\
&\qquad p = p_u + \frac{1}{2}(\alpha-1)(3\alpha-1)\,\rho_u s^2, \\
&\qquad v = 0; \\
&r > r_f : \\
&\qquad \rho = \rho_u, \\
&\qquad p = p_u + 2\alpha(\alpha-1)\left(1 - \frac{\alpha-1}{4\alpha}\left(\frac{r_f}{r}\right)^3\right)\left(\frac{r_f}{r}\right)\,\rho_u s^2,
\end{aligned}
$$

$$v = s\,(\alpha - 1)\left(\frac{r_f}{r}\right)^2 .$$

Comparing the numerical results (Fig. 7) with the theoretical solution we found that while the pre- and post-flame states are captured well, the position of the flame lags the theoretical position, even after adjustment for incompressibility and resolution effects. We repeated the same experiment in 1-D spherical, 2-D cylindrical (Fig. 8) and 3-D Cartesian coordinates and obtained essentially the same results. The decrease of the flame speed is due to the curvature in the flame front itself.

For flames where mass or thermal diffusion is essential for the flame propagation, the dependence of the flame speed on flame curvature is a known phenomenon. Curvature affects the flame speed by changing the effective diffusion, and is significant when the radius of curvature is of the order of the flame thickness. In the flame modelling literature, the infinitely thin interface assumption is often combined with a "curvature correction" - an explicitly defined reduction (for outward-propagating flames; for inward propagating flames, the curvature effects are reversed) of the flame speed to account for the thickness of the flame, which is neglected. In the flame capturing model we have the opposite situation: the true flame is much thinner than its representation by the flame capturing model. Consequently, the curvature effect is overestimated, and the flame speed is underpredicted. We do not attempt to include curvature corrections in the flame-capturing model.

Both 1-D spherical and 2-D cylindrical simulations expose the downstream variations in velocity in the case of the top-hat reaction rate; this is the same acoustic-pulse behavior we observed in planar flame simulations. It is notable that despite the acoustic pulses, the flame front remains spherical.

Figure 8 also shows the AMR grid. We used an adaptive grid to alleviate the effects of boundary conditions. The solutions in Figs. 7-8 are shown only for a small part of a the computational domain.

7. Concluding remarks

In this article we analyzed the ARD flame-capturing model proposed by Khokhlov [7]. This model extends the nonreactive flow equations by solving an additional field equation for the reaction progress variable. Flame fronts are represented by the rapid spatial change in the progress variable. The desired propagation speed and flame thickness are inputs to the model. Based on several assumptions, the numerical reaction time scale and diffusion coefficient are computed dynamically; when used in the ARD equation, these parameters nominally produce the desired flame speed and thickness.

The ARD flame capturing method is easy to implement. It is inexpensive (in memory and computational time) and reasonably robust. By design, it conserves energy and satisfies the Rankine-Hugoniot conditions across the flame. The input flame speed is a free parameter, and can be chosen dynamically based on, e.g. flow conditions, ignition or quenching conditions, thermodynamic state, simulation time, etc.

One drawback of the model is low accuracy at off-design conditions. Our measure of accuracy is how well the observed flame speed compares to the input flame speed. (As mentioned earlier, our analysis could be repeated for the flame thickness.) We showed that unless thermal expansion across the flame is negligible, systematic error is apparent in the observed flame speed when the top-hat reaction rate is used. We then developed a correction to account for thermal expansion and demonstrated its effectiveness. We also showed that for a class of reaction rates including the KPP reaction rate, no corrections for thermal expansion are necessary.

The deeper implication of our analysis is that any fluid motion which distorts the flame front potentially taints the observed flame speed. In a true flame, the flame speed is affected by any fluid motion that influences the balance between diffusion and reaction. In the ARD model, such motions are violations of the assumptions under which the numerical diffusion coefficient and reaction time scale are computed — off-design conditions. The original ARD model computed the diffusion coefficient and reaction time scale assuming an incompressible, laminar, planar, shear-free flame. To the extent that these assumptions are satisfied, one can expect good results from the model. Our correction for thermal expansion on the flame profile relaxes the incompressibility assumption, as long as the other assumptions are met. So despite the correction, the cylindrical and spherical flame speed in Section 6.2 are not accurately computed because of these flames are not planar. Neither does our correction address, e.g. turbulent fluctuations (velocity fluctuations on the scale of the model flame thickness,) tangential velocity differences, or flame stretching.

Despite this drawback, we believe the ARD model has a place in the flame modelling arsenal. For those considering it, we offer the following comments:

- The ARD model is simple, and users should not expect it to outperform well-developed, more sophisticated models over a wide range of conditions. Instead, consider the ARD model as a way to reduce computational costs when the advantages of otherwise acceptable, more sophisticated models are not essential features of your simulations.
- Depending on the application, some properties of the ARD model may be more important than others. If matching the input flame thickness is a higher priority than matching the flame speed, one could repeat our approach with that as the focus. Front thickening due to thermal expansion can be reduced by calibrating the input parameters.
- Representing the flame as a diffuse interface has several consequences. The model flame is more intrusive in that it takes up a larger fraction of the domain. The diffuse representation can also make the flame more sensitive to local fluid motions and flowfield variations than a discontinuous representation. As described above, this sensitivity can ultimately lead to lower accuracy. The flame model does not account for scales less than the flame thickness, which is several times larger than the grid scale.
- Because of the drawbacks of the diffuse representation of the flame, users of the ARD model will try to choose the minimum number of grid points to resolve the flame (i.e. small b.) Consequently the interplay between the model and the truncation error of the discretized advection and diffusion operators will always be an issue. It is very difficult to achieve a highly accurate flame speed over a broad range of conditions and at low resolutions, and particular attention is needed to ensure that errors in the observed flame speed are within acceptable limits.
- While the input flame speed is arbitrary, some care should be taken when specifying a dynamically determined value. The input flame speed is usually expressed as a function of the unburned state. In a given cell, though, the available

information is the current state, which may be anywhere between unburned and burned. One strategy is to derive an analytic relationship which parameterizes the thermodynamic state as a function of reaction progress variable; then the unburned ($\phi = 0$) state can be reconstructed from the current value of ϕ. However, such analytical relationships depend on the form of the equation of state, and might not have closed-form solutions.

- One could investigate other reaction rates, $R(\phi)$. We considered only the KPP and top-hat rates, and found each had strengths and weaknesses. It would be nice to find a reaction rate which provides smooth profiles and the desired (input) travelling wave speed independent of thermal expansion, like KPP, but a (relatively) thin interface and insensitivity to noise near $\phi = 0$, like top-hat. The steep but smooth functions are preferable since they produce profiles which are less likely to be distorted by flow, and yet do not generate acoustic waves at the cell borders. Of course, the reaction rate form can be chosen to retain some properties of physical system it represents, but such properties might be lost in the simplicity of the ARD model.
- The ARD model may be implemented in an operator split or unsplit fashion; the choice will generally follow the approach of the code it is added to. In the prototype code, we observe that split and unsplit implementations can give different results when the time step is comparable to the Courant limit based on the flow velocity. As the time step is decreased, the two implementations converge to the same value. In our tests, the trend is that if the split and unsplit results agree, they are both well-resolved in time. No positive statement can be made if the results depend on the splitting, and spatial resolution is, of course, an independent issue.
  When the ARD model is implemented in a compressible flow code, there are suggestions that a particular split implementation delivers superior flame speed results compared to other split and unsplit versions. We view this as a fortuitous combination of truncation errors.

Finally, we feel a significant contribution of our work is our technique for decoupling the ARD equation from the fully coupled system. After analyzing the full system of conservation equations with thermodynamics, we developed a model for including thermal expansion effects in the isolated ARD equation; namely, we considered the dependence of the advection velocity on the reaction progress variable, $\mathbf{v}(\phi)$. This reduced the complexity of the full system to a tractable problem, more amenable to analytical approaches. Many others work with the isolated ARD equation [17, 1], but we are not aware of studies with $v(\phi)$ term. We hope this technique will bridge a gap between theorists and mathematicians and their rigor, on the one hand, and applied scientists and engineers, and their more realistic systems on the other.

Acknowledgements

This work was supported by the Department of Energy under Grant No. B341495 to the Center for Astrophysical Thermonuclear Flashes at the University of Chicago. The authors are grateful for the support of and many discussions with Bronson Messer, Alan Calder, and Alexei Khokhlov.

Appendix A: Analytical solution for isochoric fluid with top-hat reaction rate.

Let us consider the advection-reaction-diffusion equation (1), with top-hat reaction rate (3), for an isochoric fluid, e.g. with $v(\phi) = v_u = const.$ In the reference frame of the travelling wave ($v_u = -s_0$) equation (1) becomes,

$$s_0\phi_x = \kappa\phi_{xx} + \tau^{-1}R(\phi).$$

If the flame is moving to the left, the solution $\phi(x)$ is increasing with boundary conditions $\phi(-\infty) = 0$, $\phi(\infty) = 1$.

Suppose the reaction rate is non-zero on the interval $0 < x < x_1$. The solution, matching boundary conditions at $x = \pm\infty$ and continuous at $x = 0$ and $x = x_1$, is

$$\begin{aligned}
&\phi = \phi_0 e^{\frac{x}{\delta_0}}, && x < 0,\\
&\phi = \left(1 - \phi_0 - R_0\frac{x_1}{\delta_0}\right)\frac{e^{\frac{x}{\delta_0}} - 1}{e^{\frac{x_1}{\delta_0}} - 1} + \phi_0 + R_0\frac{x}{\delta_0}, && 0 < x < x_1,\\
&\phi = 1, && x > x_1,
\end{aligned}$$

where $\delta_0 = \tau s_0 = \kappa/s_0$.

The additional requirement of a continuous first derivative, $\phi'(x)$, determines the width of the reacting region, $x_1 = \delta_0/R_0$. It also determines the maximum reaction rate, R_0, which must be the root of the equation $(\phi_0 - R_0)e^{1/R_0} + R_0 = 0$. Taking these restrictions into account, we can rewrite the solution above,

$$\begin{aligned}
&\phi = \phi_0 e^{\frac{x}{\delta_0}}, && x < 0,\\
&\phi = (\phi_0 - R_0)e^{\frac{x}{\delta_0}} + R_0\left(1 + \frac{x}{\delta_0}\right), && 0 < x < x_1,\\
&\phi = 1 && x > x_1.
\end{aligned}$$

Note that the parameter R_0, which specifies the reaction rate for top-hat reaction, is a function of ϕ_0 only. In the flame capturing model we use the top-hat reaction rate (3) with $\phi_0 = 0.3$ and corresponding $R_0 \approx 0.3128$.

Appendix B: Flame speed for expanding fluid with KPP reaction rate.

We show in this appendix that the ARD equation with KPP reaction rate admits travelling wave solutions moving with all speeds $s \geq s_0 = 1$. The physically observed solutions correspond to the minimal speed $s_0 = 1$.

We start with the ARD equation expressed in the units of δ_0 and τ, in the reference frame of the unburned fluid,

$$\phi_t - \beta\phi\phi_x = \phi_{xx} + \frac{1}{4}f(\phi). \tag{B.1}$$

Here $\beta = (\alpha - 1)s/s_0 \geq 0$, and reaction term $f(\phi) \in C^1([0,1])$ is a KPP type nonlinearity, such as $f(\phi) = \phi(1-\phi)$. That is, we assume that $f(0) = f(1) = 0$, $f(\phi) > 0$ for $0 < \phi < 1$, $f'(0) = 1$ and

$$f'(0) = \max_{0\leq\phi\leq 1}\frac{f(\phi)}{\phi}. \tag{B.2}$$

In particular, this implies that $f(\phi) \leq \phi$ for $\phi > 0$.

The boundary conditions are

$$\phi(-\infty) = 1, \quad \phi(+\infty) = 0.$$

We look for travelling wave solutions of the type $\phi(t,x) = U(x - st)$, so that $U(x)$ satisfies an ODE

$$-sU' - \beta UU' = U'' + \frac{1}{4}f(U), \quad U(-\infty) = 1, \quad U(+\infty) = 0. \tag{B.3}$$

We introduce $V = -U'$ so that (B.3) becomes

$$\begin{aligned} \frac{dU}{dx} &= -V \\ \frac{dV}{dx} &= -(\beta U + s)V + \frac{1}{4}f(U). \end{aligned} \tag{B.4}$$

This system has two equilibria: $(U,V) = (0,0)$ and $(U,V) = (1,0)$. A travelling wave corresponds to a heteroclinic orbit of (B.4) that goes from the second equilibrium $(1,0)$ to the first, $(0,0)$. The linearization around $(0,0)$ gives

$$\frac{d}{dx}\begin{pmatrix} U \\ V \end{pmatrix} = A_0 \begin{pmatrix} U \\ V \end{pmatrix}, \quad A_0 = \begin{pmatrix} 0 & -1 \\ \frac{1}{4}f'(0) & -s \end{pmatrix}.$$

The eigenvalues of A_0 satisfy

$$\lambda^2 + s\lambda + \frac{1}{4}f'(0) = 0$$

and are both real and negative if $c^2 \geq f'(0) = 1$. Therefore, for a positive travelling wave $U(x-st)$ to exist, we need $s \geq 1$ so that $(0,0)$ is a stable point. The linearization around $(1,0)$ gives

$$\frac{d}{dx}\begin{pmatrix} \tilde{U} \\ \tilde{V} \end{pmatrix} = A_1 \begin{pmatrix} \tilde{U} \\ \tilde{V} \end{pmatrix}, \quad A_1 = \begin{pmatrix} 0 & -1 \\ \frac{1}{4}f'(1) & -(s+\beta) \end{pmatrix}.$$

The eigenvalues of A_1 satisfy

$$\lambda^2 + (s+\beta)\lambda + \frac{1}{4}f'(1) = 0$$

so that they have a different sign: $\lambda_1 > 0$, $\lambda_2 < 0$, as $f'(1) < 0$, and $(1,0)$ is a saddle. Note that the unstable direction $(1, -\lambda_1)$ corresponding to $\lambda_1 > 0$ lies in the second and fourth quadrants.

Let us look at the the triangle D formed by the lines $l_1 = \{V = \gamma_1 U\}$, $l_2 = \{V = \gamma_2(1-U)\}$ and the interval $l_3 = \{[0,1]\}$ on the U-axis. We check that when $s \geq 1$, and with an appropriate choice of γ_1 and $\gamma_2 \geq |\lambda_1|$ all trajectories of (B.4) point into D on the boundary ∂D if $\beta \geq 0$ and $s \geq 1$. That means that the unstable manifold of $(1,0)$ has to end at $(0,0)$ since it may not cross the boundary of the triangle: it enters the triangle at $(0,1)$ because $\gamma_2 > |\lambda_1|$. That is, U and V stay positive along a heteroclinic orbit that starts at $(1,0)$ and ends at $(0,0)$ – this is a monotonic positive travelling wave we are looking for. In particular, that will show that the minimal speed is $s_* = 1$ for all $\beta \geq 0$.

Along l_3 we have

$$\frac{dU}{dx} = 0, \quad \frac{dV}{dx} = \frac{1}{4}f(U) > 0$$

so that trajectories point upward, that is, into D. Furthermore, along l_1 we have $\dfrac{dU}{dx} = -V < 0$ and

$$\frac{dV}{dU} = s + \beta U - \frac{f(U)}{4V} = s + \beta U - \frac{f(U)}{4\gamma_1 U}.$$

That means that the trajectory points into D if the slope $\dfrac{dV}{dU} \geq \gamma_1$ along l_1. This is true if

$$s + \beta U \geq \frac{f(U)}{4\gamma_1 U} + \gamma_1 \tag{B.5}$$

for all $U \in [0, 1]$. Recall that $f(U) \leq U$, and thus (B.5) holds provided that

$$s \geq \frac{1}{4\gamma_1} + \gamma_1. \tag{B.6}$$

This is true for $s \geq 1$ and $\gamma_1 = 1/2$.

Let us check that with this choice of s and γ_1 all trajectories point into D also along l_2. Indeed we have along l_2: $\dfrac{dU}{dx} = -V < 0$ and

$$\frac{dV}{dU} = s + \beta U - \frac{f(U)}{4V} = s + \beta U - \frac{f(U)}{4\gamma_2(1-U)}.$$

That means that the trajectory points into D if the slope $\dfrac{dV}{dU} \geq -\gamma_2$ along l_1. This is the case if

$$s + \beta U - \frac{f(U)}{4\gamma_2(1-U)} \geq -\gamma_2$$

for all $U \in [0, 1]$, or, equivalently,

$$s\gamma_2 + \gamma_2^2 + \gamma_2 \beta U \geq \frac{f(U)}{4(1-U)}.$$

This is true for instance if $s \geq 1$, and $\gamma_2 \geq m_0$, where $m_0 = \inf\limits_{0 \leq U \leq 1} \dfrac{f(U)}{4(1-U)}$. In particular, we may choose $\gamma_2 \geq |\lambda_1|$. Therefore, a travelling front exists provided that $s \geq 1$ and $\beta \geq 0$. However, we have also shown that no travelling front exists for $s < 1$. Thus we have proved that the travelling front solution of (B.3) exists for all $s \geq 1$.

As in the case $\beta = 0$, the observed travelling wave speed corresponds to the smallest possible s, that is, $s = 1$, or, in physical units, to $s = s_0$. This result does not depend on the choice of $\beta > 0$, and consequently on the density ratio α between the burned and unburned fluid.

References

[1] Berestycki H 2002 The influence of advection on the propagation of fronts for reaction-diffusion equations, in *"Nonlinear PDE's in Condensed Matter and Reactive Flows"* (Berestycki H and Pomeau Y, eds.), NATO Science Series, Ser. C **589** 11

[2] Calder A C *et al* 2002 On Validating an Astrophysical Simulation Code, *Astrophys. J.* **143** 201

[3] Colella P and Woodward P 1984 The Piecewise Parabolic Method (PPM) for Gas-Dynamical Simulations, *J. Comput. Phys.* **54**(1) 174

[4] Fryxell B *et al* 2000 FLASH: An Adaptive Mesh Hydrodynamics Code for Modeling Astrophysical Thermonuclear Flashes, *Astrophys. J.* **131** 273

[5] Fisher R 1937 The wave of advance of advantageous genes, *Ann. Eugenics* **7** 355
[6] Kerstein A, Ashurst W T and Williams F A 1988 Field equation for interface propagation in an unsteady homogeneous flow field, *Phys. Rev. A* **37** 2728
[7] Khokhlov A M 1995 Propagation of turbulent flames in supernovae, *Astrophys. J.* **449** 695
[8] Kolmogorov A N, Petrovskii I G and Piskunov N S 1937 Étude del'équation de la chaleurde matière et son application à unproblème biologique, *Bull. Moskov. Gos. Univ. Mat. Mekh.* **1** 1 (see [10] pp. 105-130 for an English transl.)
[9] Osher S and Fedkiw R 2003 *Level set methods and dynamic implicit surfaces* (New York: Springer-Verlag)
[10] Pelcé P, Ed. 1988 *Dynamics of curved fronts* (Academic Press)
[11] Rhee C J, Talbot L and Sethian J A 1995 Dynamical behavior of a premixed turbulent open V-flame, *J. Fluis. Mech.* **300** 87
[12] Sethian J A 1996, 1999 *Level set methods and fast marching methods* (Cambridge University Press)
[13] Smiljanovski V, Moser V and Klein R 1997 A capturing-tracking hybrid scheme for deflagration discontinuities, *Combust. theory and mod.* **1** 183
[14] Strang G 1968 On Construction and Comparison of Difference Schemes, *SIAM J. Num. Anal.* **5**(3) 506
[15] Srtrikwerda J C 1989 *Finite Difference Schemes and partial differential equations* (New York: Chapma & Hall)
[16] Timmes F X and Woosley S E 1992 The conductive propagation of nuclear flames. I - Degenerate C + O and O + Ne + Mg white dwarfs, *Astrophys. J.* **396** 649
[17] Xin J 2000 Front propagation in heterogeneous media *SIAM Rev.* **42** 161
[18] Zeldovich Ya B, Barenblatt G I, Librovich V B and Makhviladze G M *The Mathematical Theory of Combustion and Explosions,* Translated from the Russian by Donald H. McNeill. Consultants Bureau [Plenum], New York, 1985